Powder Technology 457 (2025) 120870

Contents lists available at ScienceDirect

Powder Technology

journal homepage: www.journals.elsevier.com/powder-technology

Vertical tubes in bubbling fluidized beds: A magnetic resonance imaging study of particle and bubble behavior

Hannah S. Rennebaum [a], Christoph R. Müller [b], Alexander Penn [a,b,c,*]

[a] Institute of Process Imaging, Hamburg University of Technology, Hamburg, Germany
[b] Department of Mechanical and Process Engineering, ETH Zurich, Zurich, Switzerland
[c] Institute for Biomedical Engineering, ETH Zurich and University of Zurich, Zurich, Switzerland

GRAPHICAL ABSTRACT

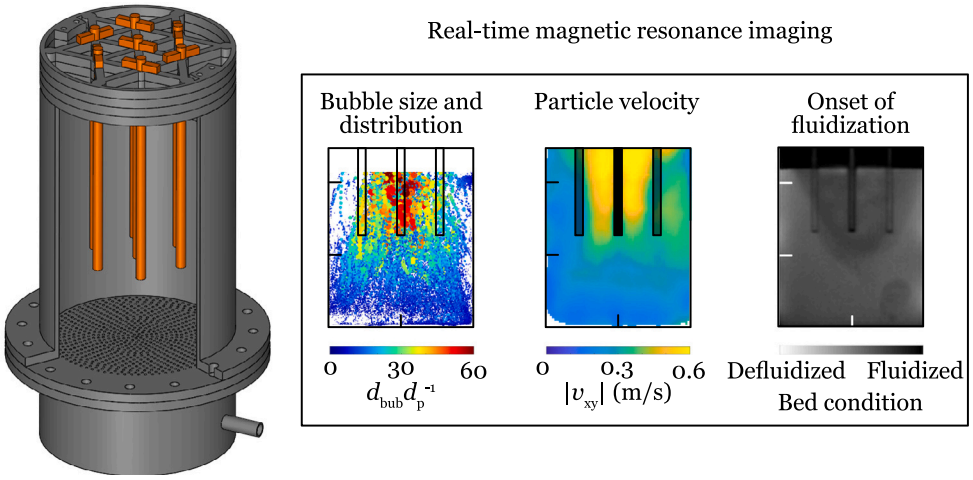

HIGHLIGHTS

- The effect of vertical tubes in bubbling fluidized beds was investigated.
- Particle velocities and bubble behavior were studied with real-time MRI.
- Vertical tubes homogenize the bubble size and the radial bubble distribution.
- Gas channeling along the vertical tubes was observed.
- Vertical tubes were found to reduce the average particle velocity fluctuation in the bed.

ARTICLE INFO

Keywords:
Fluidized beds
Magnetic resonance imaging
Vertical tubes
Bubble dynamics

ABSTRACT

Vertical tubes are commonly introduced into fluidized bed reactors, for example, to promote heat exchange. It has been shown previously that such vertical tubes affect the bed hydrodynamics, however, it is still unclear (a) whether vertical tubes cause gas channeling along the tubes and (b) how these internals affect the motion of the particulate phase within the bed. In this work, we used real-time magnetic resonance imaging (MRI) to study the influence of vertical tubes of varying lengths and diameters on the bed hydrodynamics and gas

* Corresponding author at: Institute of Process Imaging, Hamburg University of Technology, Hamburg, Germany.
E-mail address: alexander.penn@tuhh.de (A. Penn).

https://doi.org/10.1016/j.powtec.2025.120870
Received 20 September 2024; Received in revised form 10 February 2025; Accepted 28 February 2025
Available online 8 March 2025

bubble behavior. Spatially and temporally resolved MRI measurements of the local particle concentration, particle velocity, as well as fluidization sensitive measurements were carried out. Local particle concentration measurements show that vertical tubes do reduce the average size of gas bubbles in the bed and lead to a more homogeneous radial distribution of the gas bubbles. In addition, we find that tubes cause axial gas channeling, which might decrease the heat transfer between the bed and the tubes. Fluidization sensitive MRI measurements show that long tubes starting from the distributor plate homogenize the fluidization. Vertical tubes reduce the mean particle velocity compared to a fluidized bed without internals. The findings presented in this work might help to design more efficient internal geometries and provide a dataset that can be used to validate numerical simulations.

1. Introduction

Fluidized beds are well known for their high heat and mass transfer rates, making them a favorable reactor type for various industrial applications, such as food and pharmaceutical production, energy conversion, combustion, and highly endo- and exothermic reactions [1]. In industrial applications, internals such as baffles and heat exchanger tubes are commonly introduced into fluidized beds to improve the process efficiency [2]. Baffles have further been shown to reduce gas bubble growth, resulting in a reduced average bubble diameter [3]. Heat exchange tubes, whether vertical or horizontal, are often installed to control the temperature within the fluidized bed [4]. To design such internals (e.g. in terms of diameter, length, and arrangement) it is essential to determine their influence on the hydrodynamics of fluidized beds. This includes measurements of the phase distribution and particle velocity, but also the detection of dead zones and channeling.

Traditionally, information about the hydrodynamics of fluidized beds has been measured using intrusive probes such as pressure sensors [5], capacitance probes [6], and optical probes [7,8]. However, probes only provide single point measurements and lack spatially resolved information [9]. Additionally, these probes might disturb the hydrodynamics within the fluidized bed. Yet, obtaining information about particle phase distribution and particle velocity in three-dimensional fluidized beds is challenging due to the optical opacity of these systems. Pseudo-2D setups can overcome the optical challenges of three-dimensional fluidized beds. In a pseudo-2D fluidized bed, the third dimension is reduced significantly to allow optical accessibility throughout the entire bed [10]. However, pseudo-2D fluidized beds have other limitations, as they are for example dominated by wall effects [11], leading to measurements that may not fully represent a three-dimensional fluidized bed behavior. Therefore, tomographic techniques such as X-ray [12], magnetic resonance imaging (MRI) [13–17], and others [18], provide non-invasive measurements of three-dimensional flow systems.

One drawback of MRI is its comparably low temporal resolution, which can be improved by using scan acceleration, such as parallel imaging [19]. For time-averaged velocimetry measurements of single slices in fluidized beds the temporal resolution was until recently, in the order of minutes [14], which was insufficient to measure particle velocities in real-time. Penn et al. [16] were able to significantly reduce the acquisition time by adapting the radiofrequency detector design, the efficiency of the sequences to the geometry and the signal properties of the fluidized bed, thus enabling real-time MRI of fluidized beds. The real-time sequences allow to capture images at temporal resolution high enough to image the instantaneous position of gas bubbles in the fluidized bed. Real-time MRI has been used to characterize the gas bubble behavior and particle velocity in fluidized beds [17], to measure the effect of small amounts of injected liquid in a fluidized bed [20], to study single bubbles injected into an incipient fluidized bed [21], and to investigate the impact of various baffle designs on the fluidized bed hydrodynamics [3]. Compared to other tomographic techniques such as X-ray, MRI enables direct measurements of the velocities of fluids and granular media and allows temperature measurements [22].

The influence of horizontal tubes on the hydrodynamics of fluidized beds has been previously studied by Penn et al. [23]. In the wake region of horizontal tubes, the size and the number of bubbles, and the particle velocity are reduced. Directly below the inserted tube, the bubble formation rate is increased. In various studies, the impact of vertical tubes on the hydrodynamics and the heat transfer in fluidized beds was investigated using tomographic techniques and probes. The heat transfer coefficient in fluidized beds with a vertical tube was investigated experimentally using heat transfer probes [24,25] showing that larger tube diameters are advantageous as they lead to increased heat transfer coefficients. To investigate the hydrodynamics in fluidized beds, Maurer et al. [26] used ultra-fast X-ray tomography to show that vertical tubes reduce the average bubble volume and increase the bubble surface area through the elongation and roughening of the bubbles. Vertical tubes narrow and thus homogenize the distribution of the hydraulic bubble diameter, which is defined as four times a bubble's area divided by its perimeter, which accounts for both the outer surface of the bubble and the interfacial area between the bubble and the vertical tubes. Additionally, vertical tubes reduce the bubble rising velocity by approximately 20%. Taofeeq et al. [27] investigated the effect of vertical tubes on the bubble frequency, local gas holdup, and heat transfer coefficient in fluidized beds using optical and temperature probes. The authors found that vertical tubes stabilize the radial position of the bubbles by inhibiting their movement towards the center of the bed and improved the heat transfer by increasing the local gas holdup and bubble frequency. A higher bubble frequency allows a frequent replacement of the solid layer surrounding the heating surface. Schillinger et al. [28] demonstrated with X-ray tomography that the column size has a minor effect on the mean bubble size and rise velocity in fluidized beds that contain vertical tubes. This finding indicates a simplified scale-up process for fluidized beds containing vertical tubes, from pilot to industrial-scale plants. Two different geometric arrangements of the vertical tubes, square and circular, showed almost no effect on the bubble diameter and rise velocity. Although the impact of vertical tubes on bubble size, number, and distribution has been extensively studied, it remains unclear how vertical internals in fluidized beds affect particle velocity and the formation of gas channeling along the tubes.

In this work, the fluidization hydrodynamics and gas bubble behavior in fluidized beds with vertical tubes of different diameters and lengths was studied using real-time MRI. The analysis covers particle velocity, gas bubble behavior, channeling, and fluidization status comparing them with a fluidized bed without internals. The measurements show that vertical tubes reduce the average bubble size and cause axial channeling.

2. Methods

2.1. Fluidized bed

A fluidized bed model (Fig. 1) with an inner diameter, D_{bed}, of 190 mm and a height of 280 mm, made from an acrylic cylinder with a thickness of 5 mm, was used for all experiments performed. Compressed air was injected into a wind box with a diameter of 190 mm and a height of 150 mm, which was connected to the fluidized bed by a distributor plate. An acrylic distributor plate of 10 mm thickness and with 6416 laser-cut holes of 0.5 mm diameter was used to homogenize the inflowing air. The airflow was controlled using a mass flow controller

(F-203AV, Bronkhorst High-Tech B.V.). The pressure drop across the bed was measured under defluidizing conditions in that the superficial gas velocities (U_0) were progressively decreased using a pressure sensor connected to LabView (National Instrument Corporation) to determine the minimum fluidization velocity (U_{mf}).

The fluidized bed was filled up to a static bed height of 210 mm with MRI-detectable agar-particles filled with medium-chain triglyceride (MCT) oil. The spherical particles with a diameter, d_p, of 1.02 ± 0.12 mm and a density of $1040\,kg/m^3$ belong to the Geldart group B. More detailed information on particle properties is provided by Penn et al. [16]. Hexagonal arrays of seven vertical acrylic tubes with a diameter, d_{tube}, of 10 and 20 mm, hereafter referred to as tubes with a small and large diameter, respectively, were introduced into the fluidized bed. An acrylic holder consisting of four 10 mm thick plates glued to each other was used to hold the tubes in the fluidized bed. Three different separation distances, h_{tube}, between the distributor plate and the tubes of 0, 60, and 120 mm were investigated. The tubes were arranged with a central tube circumferentially surrounded by six tubes with center distances of 49 mm (Fig. 1a). All vertical tubes were filled with the same MRI-detectable particles described above to minimize artifacts caused by varying magnetic susceptibility. Each combination was measured with different superficial gas velocities of 0, 1, 1.25, 1.5, and 2 times the minimum fluidization velocity.

2.2. Magnetic resonance imaging

All measurements in this study were performed on a clinical 3 T human MRI system (Philips Achieva, Philips Healthcare, The Netherlands). Data were acquired with a custom-built 16-channel radiofrequency receiver array [16] and reconstructed using the MATLAB MRecon library (Gyrotools LLC, Zurich, Switzerland). Time series of two-dimensional MRI images of both horizontal and vertical orientation were acquired from the three-dimensional bed. MRI measurements of (a) particle density, (b) particle velocity measurements, and (c) local fluidization at the minimum fluidization velocity were performed. In the vertical direction, two imaging planes were recorded, at a relative angle of 30° to one another (Fig. 1). In the horizontal direction, one imaging plane at a height of 150 mm above the distributor plate was acquired. To reduce the data acquisition time for the particle density and velocity measurements, parallel imaging [29] combined with time-efficient single-shot echo planar imaging (EPI) pulse sequences [30] were used. The sequence of particle velocity measurements was previously employed by Boyce et al. [31] to determine particle velocities in the wake and top of single rising bubbles. These velocities were put in relation to the bubble rise velocity determined from spin density measurements of the same dataset, which enables to validate the accuracy of the MRI-based particle velocity measurements. For the fluidization sensitive MRI, recorded data from 9 s were averaged in time. The fluidization sensitive MRI measurements presented here are similar to the concept of intravoxel incoherent motion (IVIM) imaging, in which areas with a high diffusion coefficient appear darker compared to areas with a low diffusion coefficient. In the measurements presented here, areas in which particles move incoherently (i.e. diffusion-like), as it is the case for fluidized particles, are subject to a diffusion-attenuation of the MRI signal. The prephaser and readout gradient in the frequency encoding direction act as the bipolar "diffusion" gradient. The MRI methods used in this work are described in more detail by Penn et al. [16]. In Table 1, the experimental parameters of the MRI measurements are listed.

2.3. Data processing

MRI images were processed and analyzed using MATLAB. For the local particle concentration and the particle velocity measurements, the pixels were automatically assigned, based on the pixel intensity, to the gas phase and the particles. This allocation based on the signal

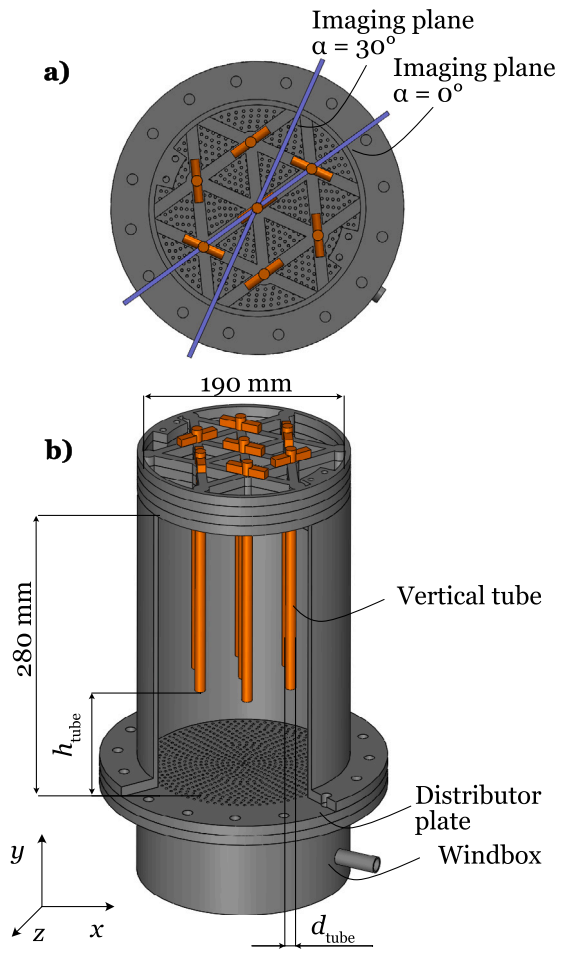

Fig. 1. Schematics of the fluidized bed model from both (a) a top view and (b) a side cut from the front. The separation distance, h_{tube}, between the distributor plate and the tubes is 0, 60, and 120 mm. In vertical orientation, two imaging planes are recorded, rotated at a relative angle of 30° to one another.

intensity of a pixel was determined by a spatially-dependent threshold. The spatially-dependent threshold results from the spatially-dependent average signal intensity of the measurement of the static bed without gas volume flow. In contrast to previous work [3], pixels below 60% of the spatially-dependent average signal were allocated to the gas phase, as this value proved to be more stable for the datasets analyzed in this study. A sensitivity analysis of the threshold percentage value can be found in the supplementary material (Fig. S1). Pixels inside the tubes and erupted bubbles were excluded from the analysis. Bubbles with an area of $A_{bub} < 2\pi\Delta x\Delta y$, where Δx and Δy are the spatial resolution in the x-direction and the y-direction, respectively, were excluded from the data evaluation, as well. If a bubble was detected on both sides of the tube, it was assumed to surround the tube and therefore counted as one bubble.

Local particle concentration measurements in the vertical direction were carried out to determine the equivalent bubble diameter (Eq. (1)), denoted as d_{bub}, based on the measured bubble area, A_{bub}.

$$d_{bub} = \sqrt{\frac{4A_{bub}}{\pi}} \tag{1}$$

In the horizontal direction, the local particle concentration measurements were used to evaluate if vertical tubes cause channeling of gas bubbles along the tubes. A brightness adjustment with setting pixel intensities above the 99% percentile to the maximum was conducted to prevent particle concentrations in fluidized bed with gas flow from being systematically underestimated. This effect occurs when excited

Table 1
Experimental parameters for the local particle concentration, particle velocity, and fluidization sensitive MRI measurements.

Measurement type	Vertical			Horizontal
	Local particle concentration	Particle velocity	Fluidization sensitive	Local particle concentration
Number of recorded frames per experiment	1000	500	1	200
Field of view [mm]	205 × 326 (x × y-direction)		200 × 290 (x × y-direction)	200 × 200 (x × z-direction)
Temporal resolution [ms]	8	23	9000	83
Spatial resolution [mm]	3 × 3 × 10 (x × y × z-direction)	3 × 5 × 15	2.5 × 2.5 × 10	3 × 5 × 15 (x × z × y-direction)
Flip angle [°]	15			
Repetition time t_R [ms]	8	8	2	2
Echo time t_E [ms]	1	2	1	1
Velocity encoding [m/s]	–	1.5 in x and y-direction	–	–
Field of flow				

material leaves the field of view and unexcited material enters, which is a phenomenon known as inflow artifacts. An example of the brightness adjustment is shown in the supplementary material (Fig. S2). A bubble probability, $\mathbb{P}(\text{bub})$ (Eq. (2)), which gives the time-averaged probability of gas bubbles to be located in each pixel of the bed, is calculated from the time-averaged particle concentration as a function of the distance from the center of the nearest tube, $\tilde{r}$.

$$\mathbb{P}(\text{bub}) = 1 - \frac{I_{SD}(\tilde{r})}{I_{SD,0}(\tilde{r})} \tag{2}$$

The bubble probability is calculated by one minus the ratio of the average particle concentration of a measurement with gas flow, $I_{SD}(\tilde{r})$, divided by the average particle concentration at the same position and setup without a gas flow, $I_{SD,0}(\tilde{r})$. To gain the same evaluation for the fluidized bed without internals, virtual centers are assumed to be located at the same positions as the center of the tubes with a large diameter. The definition of $\mathbb{P}(\text{bub})$ used here is robust against a spatially varying sensitivity of the detector array. It is important to note, however, that other effects than gas concentration might influence the signal intensity $I_{SD}(\tilde{r})$ observed in the MRI images. These effects include (a) intra-voxel incoherent motion of the particles during the acquisition time, which leads to a signal attenuation and (b) inflow artifacts, which can lead to a signal increase.

From the particle velocity measurements the average in-plane velocity (Eq. (3)), $|v_{xy}|$, is calculated, where v_x is the measured velocity in x-direction and v_y is the measured velocity in y-direction.

$$|v_{xy}| = \frac{1}{N}\sum_{i=1}^{N}\sqrt{v_{x_i}^2 + v_{y_i}^2} \tag{3}$$

3. Results and discussion

3.1. Bubble size and distribution

Fig. 2 shows the spatial distribution of gas bubbles gained from MRI measurements of the local particle concentration in vertical direction. Examplary particle concentration measurement for varying superficial gas velocities and tube configurations can be found in the supplementary material (Fig. S3). The segmented bubbles are color-coded by size and collected at their center of mass in (a) for the fluidized bed without tubes, in (b) for tubes with a small and in (c) for tubes with a large diameter (Fig. 2). Here and for the following evaluations, the two recorded vertical orientations with a relative angle of 30° to one another (Fig. 1a) have been combined to increase the database and reduce directional effects in the evaluation. The two recorded vertical orientations are shown separately in the supplementary material (Fig. S4) for a superficial gas velocity of 2 U_{mf}. Our findings show that the average bubble size increases with distance from the distributor plate for all investigated configurations, with the largest bubbles observed at the top of the fluidized bed. As the bubble size increases, the number of bubbles decreases due to bubble coalescence. This has already been observed previously using MRI [3,23]. For a quantitative comparison, the bubble diameter is additionally plotted against the bed height in Fig. 3a for a superficial gas velocity of 1.5 and in 3b for 2 U_{mf}.

We find that vertical tubes reduce the average equivalent bubble diameter. Tubes with a larger diameter have a more pronounced effect in reducing the average bubble diameter compared to smaller tubes, while the length of the tubes has no significant influence on the average bubble diameter. Tubes with a larger diameter reduce the average bubble diameter for a superficial gas velocity of 2 U_{mf} by up to 40% and smaller tubes by up to 35% compared to the fluidized bed without internals. For lower superficial gas velocities of 1.25 or 1.5 U_{mf}, the average bubble size is also reduced by the introduction of vertical tubes, but less pronounced (Fig. 3a and S7). The reduction in average equivalent bubble diameter, which becomes more pronounced at higher superficial gas velocities with the introduction of vertical tubes, was also reported by Maurer et al. [26] and Rüdisüli et al. [32]. Maurer et al. conducted measurements using X-ray imaging of single horizontal slices across a wide range of heights (13 to 48 cm) and superficial gas velocities (1.5 to 4 U_{mf}). Their setup had similar dimensions to the one in our study and particles classified between Geldart groups A and B. The percentage reduction in equivalent bubble diameter observed by Maurer et al. aligns in scale with the results obtained here. Building up on these findings, we examined the equivalent bubble diameter at smaller heights and found that all setups exhibited a similar behavior regarding bubble size up to a height of 0.4 D_{bed}. At these heights, the introduction of tubes had no effect on the equivalent bubble diameter.

Compared to Maurer et al. our study additionally investigated the impact of tube design on the bubble size by varying the diameter and length of the tubes. Rüdisüli et al. also studied the influence of tube diameter but provided data only for a single height, using optical probes and pressure fluctuation measurements. In contrast to our findings, they reported a stronger bubble size reduction effect for smaller tube diameters. Potential reasons for this are the use of a bank of tubes with U-shaped endings that connect two tubes at their ends, thereby increasing the likelihood of bubble-splitting events. Additionally, while we kept the total number of tubes constant, the smaller diameter resulted in an increased number of tubes in the bank, from 12 for the larger diameter to 37 for the smaller.

Fig. 2 shows the homogeneity of the radial bubble distribution in different fluidized bed configurations. In the fluidized bed without internals, the bubbles tend to migrate towards the bed center while rising through the bed. This inhomogeneous bubble distribution has been described to result in a wider distribution of the gas residence times [33] and to affect the gas–solid contacting as well as the transport processes within the fluidized bed [34]. Our measurements show that the presence of vertical tubes homogenizes the radial bubble distribution across all studied tube diameters and lengths. This finding confirms and details the finding of Taofeeq et al. [27], who found a more

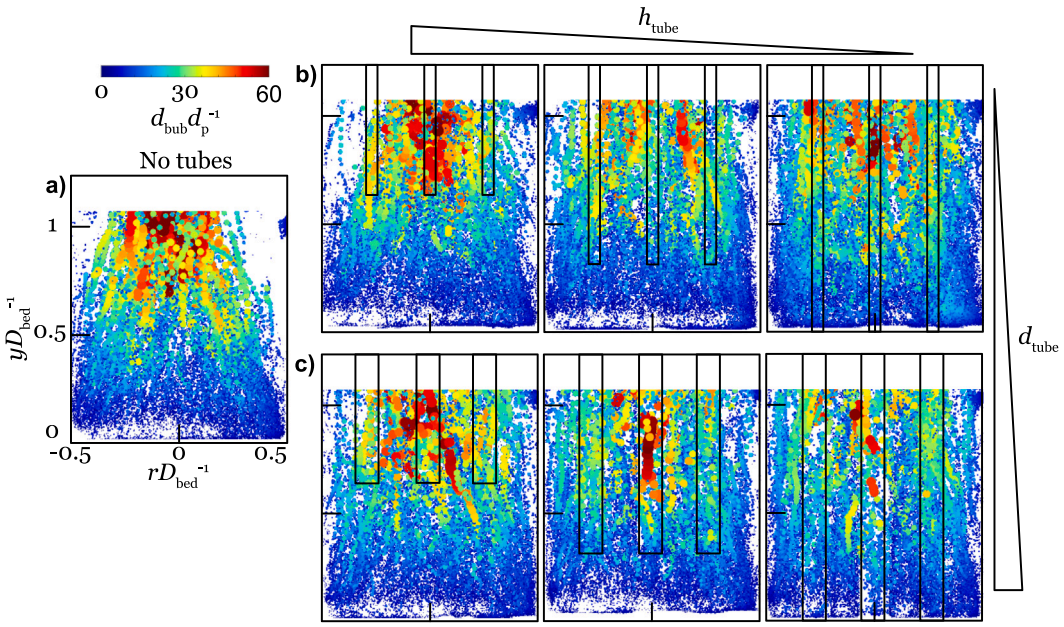

Fig. 2. Spatial distribution of gas bubbles for a measurement with a superficial gas velocity of 2 U_{mf} determined from 2000 recorded frames. Data were combined from two different data sets from the same setup and settings with a rotation at a relative angle of 30° to one another. Each bubble detected in the image time series depicted as a dot in the frame. The position of each dot corresponds to the center of mass of the corresponding bubble, while the color and size of the dot represents the equivalent bubble diameter. In (a), the measurement shows the fluidized bed without internals. In (b) and (c), measurements with a fluidized bed containing vertical tubes of a diameter of 10 mm and 20 mm, respectively, are shown. The separation distances to the distributor plate are 120, 60, and 0 mm from left to right. Respective figures for a superficial gas velocity of 1.25 and 1.5 U_{mf} can be found in the supplementary material (Fig. S5 and S6).

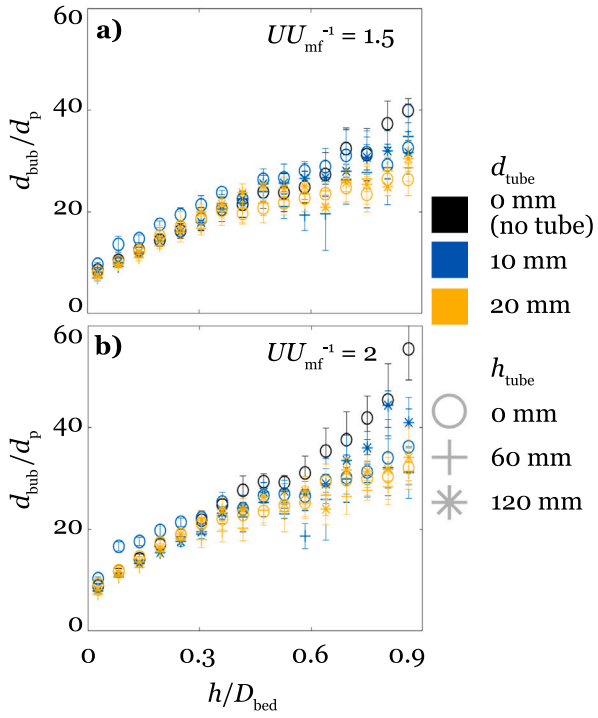

Fig. 3. Average equivalent bubble diameter over bed height for superficial gas velocity of (a) 1.5 U_{mf} and (b) 2 U_{mf}. The marker color specifies the tube diameter, and the marker shape the separation distance between the tube and the distributor plate. The figure for a superficial gas velocity of 1.25 U_{mf} is shown in the supplementary material (Fig. S7). Error bars were calculated from the standard deviation by dividing each dataset (0 and 30°) into two part with 500 frames.

homogeneous radial bubble distribution for fluidized beds with vertical tubes. Our measurements indicate increasing homogeneity of radial bubble distribution with larger tube diameters and lengths.

Fig. 4 shows the bubble size distribution within fluidized bed with vertical tube internals $N_{bub,I}$, normalized by the bubble size distribution of the bed without internals $N_{bub,0}$. Ratios above one indicate a greater number of bubbles of a given diameter within the fluidized bed containing tubes, while ratios below one signify fewer bubbles compared to the fluidized bed without internals. The number of small bubbles is higher within the fluidized bed with vertical tubes compared to the bed without internals. This holds for all investigated tube diameters and lengths. Moreover, the number of larger bubbles is significantly reduced in fluidized beds containing vertical tubes. These trends can be observed for all investigated superficial gas velocities. No clear influence of the length of the tube on the reduction of large bubbles can be found.

3.2. Gas channeling in the vicinity of the tubes

Image time series of local particle concentration measurements (Fig. 5a) in the horizontal direction are used to evaluate whether vertical tubes cause gas channeling in their vicinity. Gas channeling occurs in fluidized beds when the gas injected follows preferential pathways. Channeling reduces the particle–gas contact area and the gas residence time. Consequently, the mass transfer between the particles and the gas is decreased. Moreover, channeling can cause dead zones leading to temperature gradients within the fluidized bed, which can affect the catalyst activity and the product quality [35]. Gas channeling in the vicinity of the tubes could lead to tube insulation, in turn reducing heat transfer between the tubes and the granular medium. To detect channeling in the beds studied here, a position dependent bubble probability $\mathbb{P}$(bub) was calculated from the MR image time series as a function of the distance from the nearest tube $\tilde{r}$ (Eq. (2)). All bubble probabilities of pixels with a given distance, $\tilde{r}$, are summed and plotted in Fig. 5c–f for different tube geometries and flow conditions. Higher bubble probabilities can be observed in the vicinity of the vertical tubes

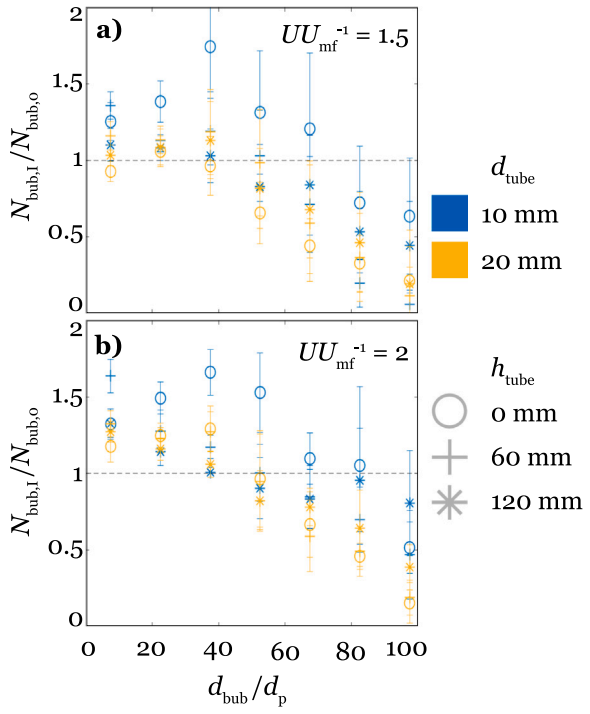

Fig. 4. The effect of vertical tubes within a fluidized bed on the bubble size distribution. The dashed horizontal line at $\frac{N_{bub,I}}{N_{bub,0}} = 1$ represents the gas bubble size distribution of a bed without vertical tubes. Superficial gas velocities of (a) 1.5 U_{mf} and (b) 2 U_{mf} are shown. The marker color specifies the tube diameter, and the marker shape the separation distance between the tube and the distributor plate. The figure for a superficial gas velocity of 1.25 U_{mf} is shown in the supplementary material(Fig. S8). The sample sizes of the detected bubbles in each diameter range are collected in the supplementary material (Tab. S2 and S3). Error bars were calculated with the Gaussian error propagation law by dividing each dataset (0 and 30°) into two part with 500 frames.

compared to the rest of the fluidized bed, indicating gas channeling. An MRI measurement without gas flow was used as a reference to account for the spatially varying sensitivity of the MRI detector elements. The vertical dotted lines at $\frac{\tilde{r}}{d_p} = 5$ and $\frac{\tilde{r}}{d_p} = 10$ represent the edges of the small and the large tubes, respectively. Data points within the tube are excluded from the evaluation. For the fluidized bed without internals, virtual tubes are positioned at the same centers as those of the tubes with the large diameter. In Fig. 5c and d, the bubble probabilities for tubes of different diameters and, in Fig. 5e and f, for tubes of different lengths are compared for a superficial gas velocity of 1.5 (Fig. 5c and e) and 2 U_{mf} (Fig. 5d and f). To visualize the distances to the nearest tube's center within the fluidized bed, distances are collected in Fig. 5b. Distances of 28 mm and more occur only at the edge of the fluidized bed and are less relevant in the assessment of gas channeling.

For a superficial gas velocity of 1.5 U_{mf} (Fig. 5c and e), the bubble probability remains constant for the fluidized bed without internals within a distance range of 0 to 25 mm from the nearest virtual tube's center indicating a uniform bubble probability. For distances greater than 25 mm the bubble probability decreases as fewer bubbles can be found close to the edge of the fluidized bed compared to the center [3]. This finding is in agreement with the spatial distribution of gas bubbles shown in Fig. 2, where a concentration of gas bubbles can be observed in the center of the fluidized bed. Introducing vertical tubes increases the bubble probability in the vicinity of the tubes, indicating channeling for both investigated diameters of 10 or 20 mm for superficial gas velocities of 1.5 and 2 U_{mf}. Channeling is more pronounced for tubes with larger diameter. A potential explanation for the observed gas channeling could be the lower packing density in the vicinity of a tube, which reduces the mechanical resistance and creates preferential paths through the fluidized bed. Additionally, tubes obstruct the incoming airflow, redirecting it to the surrounding area and increasing nearby the air volume. At larger $\tilde{r}$, the bubble probabilities for the system that contains tubes remain higher compared to the setup without internals. This is attributed to a slightly more uniform radial bubble distribution within these systems (Fig. 2), resulting in a higher bubble concentration at the edge of the fluidized bed.

In Fig. 5e and f, the bubble probability is plotted over the distance from the nearest tube's center for different lengths of the larger tube (tube diameter of 20 mm), compared to the fluidized bed without internals. This analysis shows that longer tubes lead to more pronounced channeling of gas bubbles along the tubes compared to shorter tubes.

3.3. Onset of fluidization at U_{mf}

MR images with fluidization contrast [16] were acquired of the fluidized bed containing tubes of small and large diameter (Fig. 6) at minimum fluidization velocity and compared to the fluidized bed without internals. The data were averaged over the two recorded vertical orientations with a relative rotation of 30° to one another. The measurements indicate in which area the fluidization starts. In the bed without internals, conical fluidized areas are observed, expanding in diameter with height. Beds containing long vertical tubes with a separation distance of 0 mm with a small diameter show a very similar behavior as the bed without internals. However, all other tube configurations showed to affect the area of fluidization. Tubes positioned at a distance from the distributor plate relocate the area of fluidization to the starting point of the tubes, caused by reduced bed cross-section due to tube insertion. At bed heights at which there is a reduced cross-section, the average gas velocity is higher than in the rest of the fluidized bed. Tubes with a small diameter maintain the conical shape of the fluidization pattern, while tubes with a large diameter widen the area of fluidization, forming a cylindrical shape. Long tubes with a large diameter homogenize the fluidization. Local fluidization can occur in the vicinity of obstacles even at U_{mf}, which might be relevant if beds are used in a fixed bed regime.

3.4. Particle velocity

A uniform particle velocity fluctuation within the fluidized bed is desired for efficient mass transfer between the gas phase and the granular medium throughout the entire volume of the fluidized bed. High velocities have been shown to lead to an increased risk for particle attrition [36]. Particle velocities for a superficial gas velocity of 2 U_{mf} are shown in Fig. 7. Data were averaged from the two recorded vertical orientations with a relative orientation of 30° to one another. Across all configurations, the highest particle velocities occur at the center and top of the fluidized bed, consistent with previous observations in fluidized beds containing baffles [3]. With one exception, the introduction of vertical tubes reduces the average particle velocity, with larger and longer tubes showing a stronger effect. Our findings indicate that for short tubes with a small diameter, the risk of particle attrition is increased compared to a fluidized bed without internals due to a higher mean particle velocity.

In Fig. 8, the temporally averaged velocities for the experiments conducted at 2 U_{mf} are shown separately for the two recorded orientations within the fluidized beds with a relative angle of 30° to each other. To distinguish the different directions of velocities, the heat map is combined with a vector field representing the sum of the measured velocities. Unlike the average in-plane velocity used to create the heat map, the velocities are summed such that positive and negative components cancel each other out, rather than being combined based on their absolute magnitudes. Since the fluidized bed without tubes is rotationally symmetrical, the two recorded orientations are averaged. The fluidized bed without tubes exhibits the characteristic flow pattern

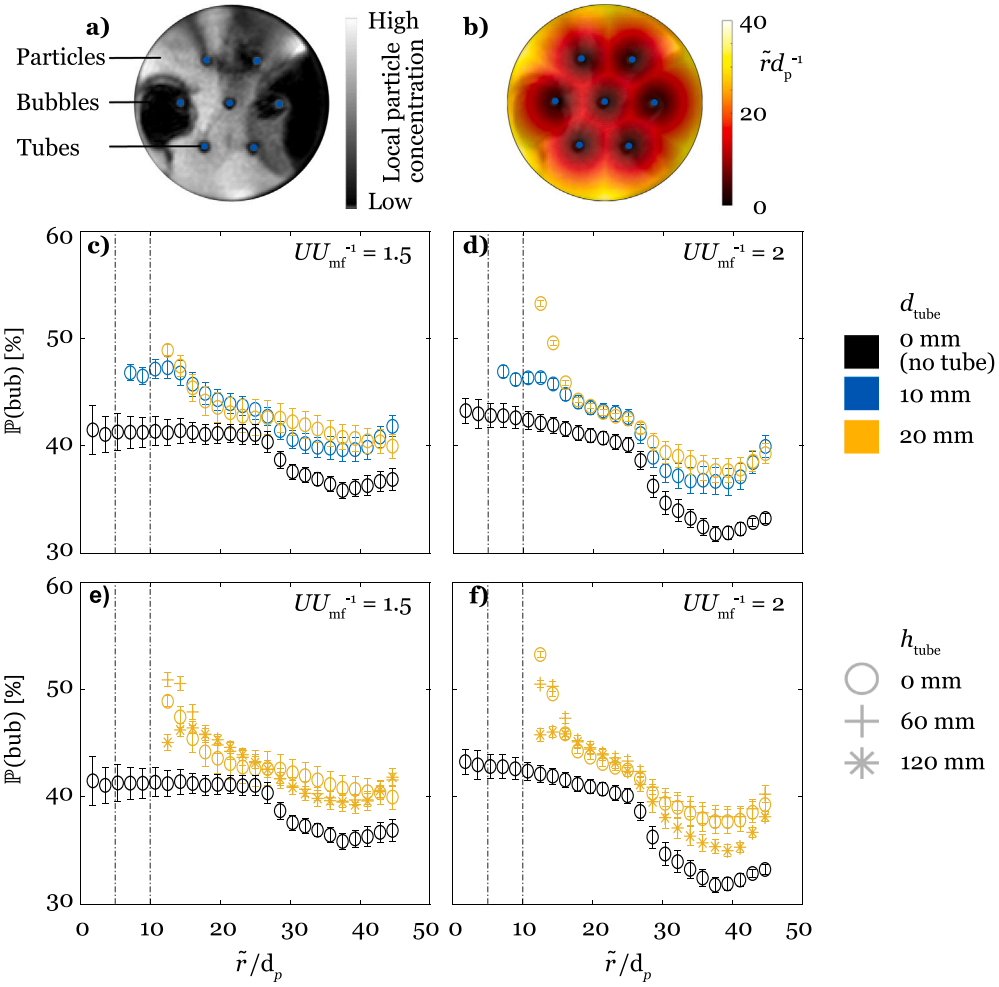

Fig. 5. (a) An arbitrary frame of a time series of horizontal MR images of local particle concentration. The blue circles show the position of the tubes. The whole time series forms the basis for the analysis shown in panels (c–f). In (b), the calculated distance from the nearest tube is plotted over the fluidized bed cross-section. Bubble probability is plotted over the distance from the nearest center of a tube. In (c) and (d), fluidized beds containing vertical tubes with a large and small diameter with a separation distance of 0 mm are compared to the fluidized bed without internals. In (e) and (f), tubes with a large diameter with varying length are compared to the fluidized bed without internals. For the measurements without internals, the virtual tube positions equal to the one in the bed with tubes with a large diameter. The measurements were conducted for a superficial gas velocity of 1.5 U_{mf} for (c) and (d) and 2 U_{mf} for (e) and (f). In diagrams (c) to (f), the marker color gives information about the tube diameter and the marker shape about the separation distance between the tube and the distributor plate. Error bars were calculated with the Gaussian error propagation law by dividing the dataset into four parts with each 125 frames.

of rising particles in the center and descending particles at the walls of the fluidized as described earlier [3,37]. In contrast, the flow pattern in the fluidized bed containing tubes is less defined. While particles generally continue to rise in the center and descend at the walls, the addition of vertical tubes creates regions with minimal particle motion, potentially reducing its efficient operation by impeding heat and mass transfer [38]. The particle velocities around the tubes show little axial movement. The measurements do not indicate any clear effects on the particle velocities based on their recorded orientation or the length of the tube. Vector fields combined with separately illustrated heat maps of the bed containing tubes with the smaller diameter can be found in the supplementary material (Fig. S10). To the best of our knowledge the impact of vertical tubes on the particle velocity within fluidized beds was investigated for the first time.

4. Conclusion

Real-time MRI was used to investigate the effect of vertical tubes of different length and diameter on the hydrodynamics of fluidized beds. Superficial gas velocities of 1, 1.25, 1.5, and 2 U_{mf} were investigated. Measurements of fluidized beds containing vertical internals were compared with the fluidized bed without internals. Particle velocity and local particle concentration measurements were conducted for all combinations of superficial gas velocities, tube diameters, and lengths. In addition, fluidization sensitive measurements were performed for a superficial gas velocity $U_0 = U_{mf}$. Our measurements show that vertical tubes reduce the average bubble size and improve the radial bubble distribution. Moreover, vertical tubes cause gas channeling along the tube. When the tubes are used to heat or cool the fluidized bed, these air pockets might provide insulation, thus decreasing heat transfer. Hence, gas channeling along vertical tubes is a disadvantage compared to horizontal tube orientation [23]. Vertical tubes with a diameter of 20 mm starting from the distributor plate can improve the fluidization homogeneity. High particle velocities at the central part of the top layer of the fluidized bed with short tubes with a small diameter increase the risk of particle attrition. Vertical tubes create regions with minimal particle motion, particularly in tubes with larger diameters.

Solid distribution, particle velocities, and temperature distribution all play a crucial role in the operation of fluidized beds with heat exchangers. Future research should focus on how tubes with different

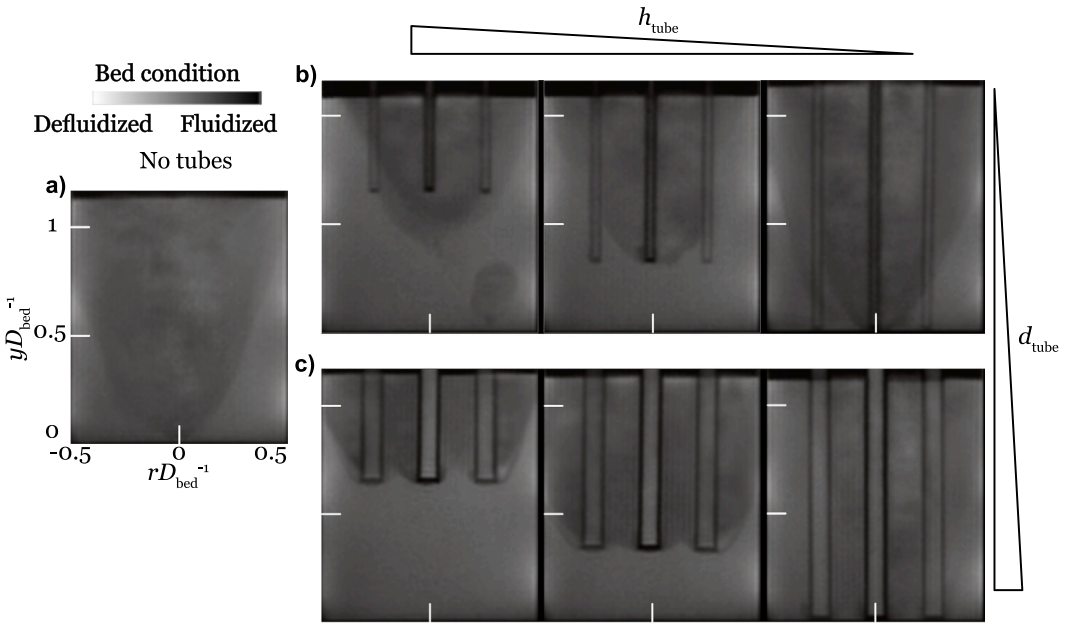

Fig. 6. Fluidization sensitive MR images for a superficial gas velocity of $U_0 = U_{mf}$ are shown. All images are averaged over the two recorded orientations with a relative angle of 30° to one another. Dark areas are fluidized and light areas are unfluidized. In (a), the measurement for the fluidized bed without internals is shown. In (b) and (c), measurements with a fluidized bed containing vertical tubes with a diameter of 10 mm and 20 mm, respectively, are shown. The distance to the distributor plate is 120, 60, and 0 mm from left to right.

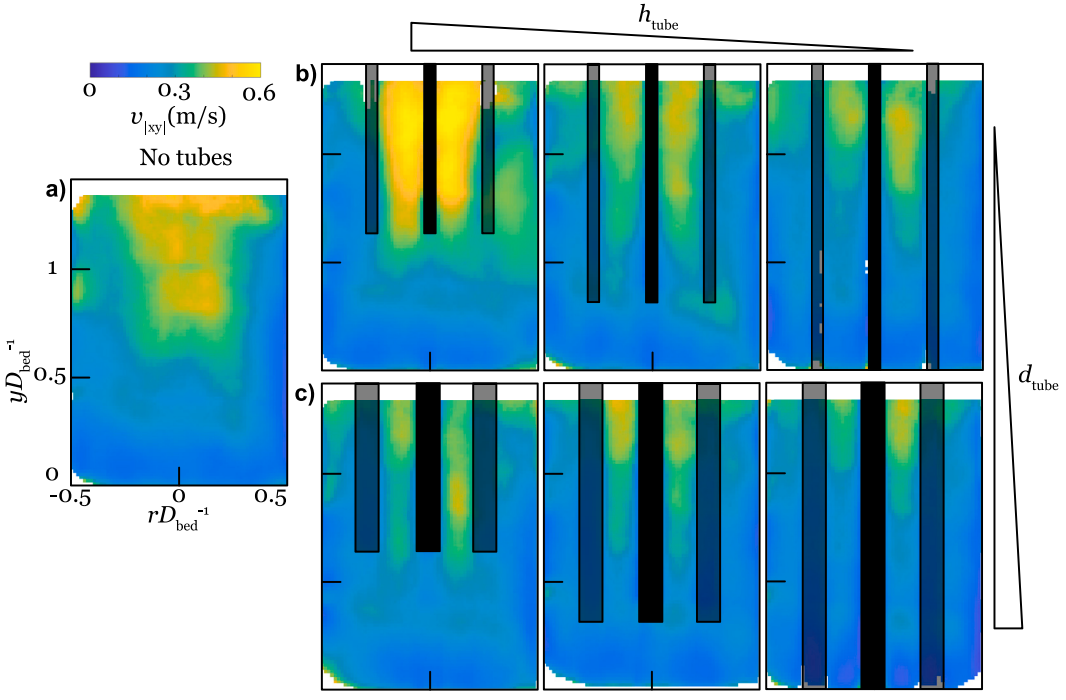

Fig. 7. Temporally averaged particle velocity for a measurement with a superficial gas velocity of 2 U_{mf} determined from 1000 recorded frames. All measurements are averaged over the two recorded orientations with a relative angle of 30° to one another. In (a), the measurement shows the fluidized bed without internals. In (b) and (c), measurements with a fluidized bed containing vertical tubes with a diameter of 10 mm and 20 mm, respectively, are shown. The distance to the distributor plate is 120, 60, and 0 mm from left to right. Respective figures for a superficial gas velocity of 1.25 and 1.5 U_{mf} can be found in the supplementary material (Fig. S11 and S12).

diameters and lengths influence the temperature distribution. MRI has demonstrated its capability for measuring both temperature and solid distributions, as previously shown for fixed beds [22]. Additionally, the relatively small height and diameter of the fluidized bed, constrained by the horizontal orientation of the MRI scanner used, can be substantially increased in future studies with the introduction of a new vertically oriented scanner, which allows sample heights of several meters and diameters of more than 300 mm.

CRediT authorship contribution statement

Hannah S. Rennebaum: Writing – review & editing, Writing – original draft, Visualization, Software, Investigation. **Christoph R. Müller:** Writing – review & editing, Methodology, Funding acquisition. **Alexander Penn:** Writing – review & editing, Methodology, Investigation, Conceptualization.

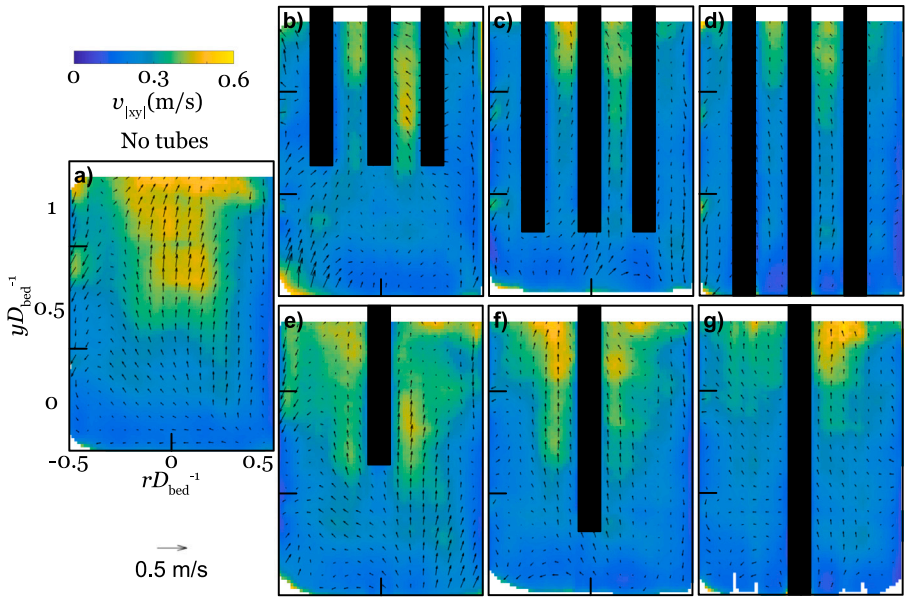

Fig. 8. Temporally averaged particle velocity overlaid by their vector field for a measurement with a superficial gas velocity of 2 U_{mf} determined from 500 recorded frames. In (a), the measurements show a fluidized bed without vertical tubes, since there are no direction-dependent effects due to internals, both orientations are still averaged. In (b) to (d), data measured with an angle of 0° are shown. In (e) to (g), the same setup with a rotation at a relative angle of 30° is shown. In (b) to (g), the measurements show the fluidized bed containing vertical tubes with a diameter of 20 mm and the separation distances to the distributor plate are 120, 60, and 0 mm from left to right.

Declaration of Generative AI and AI-assisted technologies in the writing process

This paper was copy-edited with the assistance of AI technologies as ChatGPT and Grammarly AI in order to improve clarity and readability. The authors have thoroughly checked all the proposed edits and take full responsibility for the content of this manuscript.

Declaration of competing interest

The authors declare that they have no known competing financial interests or personal relationships that could have appeared to influence the work reported in this paper.

Acknowledgments

The authors acknowledge Fanny Ludescher for her support in performing the experiments and Klaas P. Pruessmann for his contribution to the used methods in real-time MRI and the experimental setup. We would like to thank Raquel Serial and Melis Özdemir for their input during proofreading.

All data recorded and analyzed in this work are stored on a network attached storage system of Hamburg University of Technology and will be made available upon request. This work was supported by the Swiss National Science Foundation, Switzerland under grant no. 200020_182692.

Appendix A. Supplementary data

Supplementary material related to this article can be found online at https://doi.org/10.1016/j.powtec.2025.120870.

Data availability

Data will be made available on request.

References

[1] J. Grace, X. Bi, N. Ellis, Essentials of Fluidization Technology, Wiley, 2020, http://dx.doi.org/10.1002/9783527699483.

[2] Y. Jin, F. Wei, Y. Wang, Effect of internal tubes and baffles, in: W.-C. Yang (Ed.), Handbook of Fluidization and Fluid-Particle Systems, CRC Press, 2003, pp. 171–200, http://dx.doi.org/10.1201/9780203912744.

[3] H.S. Rennebaum, D.L. Brummerloh, S. Benders, A. Penn, The effect of baffles on the hydrodynamics of a gas-solid fluidized bed studied using real-time magnetic resonance imaging, Powder Technol. 432 (2024) 119114, http://dx.doi.org/10.1016/j.powtec.2023.119114.

[4] J.C. Chen, J.R. Grace, M.R. Golriz, Heat transfer in fluidized beds: design methods, Powder Technol. 150 (2) (2005) 123–132, http://dx.doi.org/10.1016/j.powtec.2004.11.035.

[5] H. Wang, A. Soria Verdugo, J. Sun, J. Wang, Y. Yang, F. Hernández Jiménez, Experimental study of bubble dynamics and flow transition recognition in a fluidized bed with wet particles, Chem. Eng. Sci. 211 (2020) 115257, http://dx.doi.org/10.1016/j.ces.2019.115257.

[6] V. Wiesendorf, J. Werther, Capacitance probes for solids volume concentration and velocity measurements in industrial fluidized bed reactors, Powder Technol. 110 (1–2) (2000) 143–157, http://dx.doi.org/10.1016/S0032-5910(99)00276-4.

[7] T. Prabu, P. Viswanathan, A. Agrawal, J. Banerjee (Eds.), Fluid mechanics and fluid power, in: Lecture Notes in Mechanical Engineering, Springer Singapore, Singapore, 2021, http://dx.doi.org/10.1007/978-981-16-0698-4.

[8] M. Rüdisüli, T.J. Schildhauer, S.M.A. Biollaz, J.R. van Ommen, Bubble characterization in a fluidized bed with vertical tubes, Ind. Eng. Chem. Res. 51 (12) (2012) 4748–4758, http://dx.doi.org/10.1021/ie2022306.

[9] M. Rüdisüli, T.J. Schildhauer, S. Biollaz, J.R. van Ommen, Measurement, monitoring and control of fluidized bed combustion and gasification, in: Fluidized Bed Technologies for Near-Zero Emission Combustion and Gasification, Elsevier, 2013, pp. 813–864, http://dx.doi.org/10.1533/9780857098801.3.813.

[10] T. Li, Y. Zhang, F. Hernández-Jiménez, Investigation of particle–wall interaction in a pseudo-2D fluidized bed using CFD-DEM simulations, Particuology 25 (2016) 10–22, http://dx.doi.org/10.1016/j.partic.2015.06.001.

[11] T. Li, P. Gopalakrishnan, R. Garg, M. Shahnam, CFD–DEM study of effect of bed thickness for bubbling fluidized beds, Particuology 10 (5) (2012) 532–541, http://dx.doi.org/10.1016/j.partic.2012.02.006.

[12] M. Bieberle, F. Barthel, U. Hampel, Ultrafast X-ray computed tomography for the analysis of gas–solid fluidized beds, Chem. Eng. J. 189–190 (2012) 356–363, http://dx.doi.org/10.1016/j.cej.2012.02.028.

[13] P.S. Fennell, J.F. Davidson, J.S. Dennis, L.F. Gladden, A.N. Hayhurst, M.D. Mantle, C.R. Müller, A.C. Rees, S.A. Scott, A.J. Sederman, A study of the mixing of solids in gas-fluidized beds, using ultra-fast MRI, Chem. Eng. Sci. 60 (7) (2005) 2085–2088, http://dx.doi.org/10.1016/j.ces.2004.11.040.

[14] C.R. Müller, D.J. Holland, A.J. Sederman, M.D. Mantle, L.F. Gladden, J.F. Davidson, Magnetic resonance imaging of fluidized beds, Powder Technol. 183 (1) (2008) 53–62, http://dx.doi.org/10.1016/j.powtec.2007.11.029.

[15] C.M. Boyce, N.P. Rice, J.F. Davidson, A.J. Sederman, J.S. Dennis, D.J. Holland, Magnetic resonance imaging of gas dynamics in the freeboard of fixed beds and bubbling fluidized beds, Chem. Eng. Sci. 147 (2016) 13–20, http://dx.doi.org/10.1016/j.ces.2016.03.005.

[16] A. Penn, T. Tsuji, D.O. Brunner, C.M. Boyce, K.P. Pruessmann, C.R. Müller, Real-time probing of granular dynamics with magnetic resonance, Sci. Adv. 3 (9) (2017) e1701879, http://dx.doi.org/10.1126/sciadv.1701879.

[17] A. Penn, C.M. Boyce, T. Kovar, T. Tsuji, K.P. Pruessmann, C.R. Müller, Real-time magnetic resonance imaging of bubble behavior and particle velocity in fluidized beds, Ind. Eng. Chem. Res. 57 (29) (2018) 9674–9682, http://dx.doi.org/10.1021/acs.iecr.8b00932.

[18] U. Hampel, L. Babout, R. Banasiak, E. Schleicher, M. Soleimani, T. Wondrak, M. Vauhkonen, T. Lähivaara, C. Tan, B. Hoyle, A. Penn, A review on fast tomographic imaging techniques and their potential application in industrial process control, Sensors (Basel, Switzerland) 22 (6) (2022) http://dx.doi.org/10.3390/s22062309.

[19] J. Hamilton, D. Franson, N. Seiberlich, Recent advances in parallel imaging for MRI, Prog. Nucl. Magn. Reson. Spectrosc. 101 (2017) 71–95, http://dx.doi.org/10.1016/j.pnmrs.2017.04.002.

[20] C.M. Boyce, A. Penn, K.P. Pruessmann, C.R. Müller, Magnetic resonance imaging of gas–solid fluidization with liquid bridging, AIChE J. 64 (8) (2018) 2958–2971, http://dx.doi.org/10.1002/aic.16036.

[21] C.M. Boyce, A. Penn, M. Lehnert, K.P. Pruessmann, C.R. Müller, Magnetic resonance imaging of single bubbles injected into incipiently fluidized beds, Chem. Eng. Sci. 200 (2019) 147–166, http://dx.doi.org/10.1016/j.ces.2019.01.047.

[22] M.R. Serial, S. Benders, P. Rotzetter, D.L. Brummerloh, J.P. Metzger, S.P. Gross, J. Nussbaum, C.R. Müller, K.P. Pruessmann, A. Penn, Temperature distribution in a gas-solid fixed bed probed by rapid magnetic resonance imaging, Chem. Eng. Sci. 269 (2023) 118457, http://dx.doi.org/10.1016/j.ces.2023.118457.

[23] A. Penn, C.M. Boyce, N. Conzelmann, G. Bezinge, K.P. Pruessmann, C.R. Müller, Real-time magnetic resonance imaging of fluidized beds with internals, Chem. Eng. Sci. 198 (2019) 117–123, http://dx.doi.org/10.1016/j.ces.2018.12.041.

[24] H. Taofeeq, M. Al-Dahhan, Investigation of the effect of vertical immersed tube diameter on heat transfer in a gas-solid fluidized bed, Int. J. Therm. Sci. 135 (2019) 546–558, http://dx.doi.org/10.1016/j.ijthermalsci.2018.10.002.

[25] T.R. White, A. Mathur, S.C. Saxena, Effect of vertical boiler tube diameter on heat transfer coefficient in gas-fluidized beds, Chem. Eng. J. 32 (1) (1986) 1–13, http://dx.doi.org/10.1016/0300-9467(86)85001-8.

[26] S. Maurer, E.C. Wagner, J.R. van Ommen, T.J. Schildhauer, S.L. Teske, S.M. Biollaz, A. Wokaun, R.F. Mudde, Influence of vertical internals on a bubbling fluidized bed characterized by X-ray tomography, Int. J. Multiph. Flow 75 (2015) 237–249, http://dx.doi.org/10.1016/j.ijmultiphaseflow.2015.06.001.

[27] H. Taofeeq, M. Al-Dahhan, Heat transfer and hydrodynamics in a gas-solid fluidized bed with vertical immersed internals, Int. J. Heat Mass Transfer 122 (2018) 229–251, http://dx.doi.org/10.1016/j.ijheatmasstransfer.2018.01.093.

[28] F. Schillinger, S. Maurer, E.C. Wagner, J.R. van Ommen, R.F. Mudde, T.J. Schildhauer, Influence of vertical heat exchanger tubes, their arrangement and the column diameter on the hydrodynamics in a gas–solid bubbling fluidized bed, Int. J. Multiph. Flow 97 (2017) 46–59, http://dx.doi.org/10.1016/j.ijmultiphaseflow.2017.07.013.

[29] K.P. Pruessmann, M. Weiger, M.B. Scheidegger, P. Boesiger, SENSE: Sensitivity encoding for fast MRI, Magn. Reson. Med. 42 (5) (1999) 952–962, http://dx.doi.org/10.1002/(SICI)1522-2594(199911)42:5<952::AID-MRM16>3.0.CO;2-S.

[30] M.K. Stehling, R. Turner, P. Mansfield, Echo-planar imaging: magnetic resonance imaging in a fraction of a second, Sci. (N. Y. N. Y.) 254 (5028) (1991) 43–50, http://dx.doi.org/10.1126/science.1925560.

[31] C.M. Boyce, A. Penn, M. Lehnert, K.P. Pruessmann, C.R. Müller, Wake volume of injected bubbles in fluidized beds: A magnetic resonance imaging velocimetry study, Powder Technol. 357 (2019) 428–435, http://dx.doi.org/10.1016/j.powtec.2019.02.021.

[32] M. Rüdisüli, T.J. Schildhauer, S.M. Biollaz, J. van Ruud Ommen, Bubble characterization in a fluidized bed by means of optical probes, Int. J. Multiph. Flow 41 (2012) 56–67, http://dx.doi.org/10.1016/j.ijmultiphaseflow.2012.01.001.

[33] J. Werther, O. Molerus, The local structure of gas fluidized beds —II. The spatial distribution of bubbles, Int. J. Multiph. Flow 1 (1) (1973) 123–138, http://dx.doi.org/10.1016/0301-9322(73)90008-6.

[34] J. Li, J. Kuipers, Gas-particle interactions in dense gas-fluidized beds, Chem. Eng. Sci. 58 (3–6) (2003) 711–718, http://dx.doi.org/10.1016/S0009-2509(02)00599-7.

[35] L.A. Briens, C.L. Briens, A. Margaritis, S.L. Cooke, M.A. Bergougnou, Characterization of channelling in multiphase systems. Application to a liquid fluidized bed of angular Biobone particles, Powder Technol. 91 (1) (1997) 1–9, http://dx.doi.org/10.1016/S0032-5910(96)03206-8.

[36] H. Zhang, J. Degrève, J. Baeyens, S.-Y. Wu, Powder attrition in gas fluidized beds, Powder Technol. 287 (2016) 1–11, http://dx.doi.org/10.1016/j.powtec.2015.08.052.

[37] Y. Li, H. Fan, X. Fan, Identify of flow patterns in bubbling fluidization, Chem. Eng. Sci. 117 (2014) 455–464, http://dx.doi.org/10.1016/j.ces.2014.07.012.

[38] J. Sánchez-Prieto, A. Soria-Verdugo, J.V. Briongos, D. Santana, Stagnant regions estimation in fluidized beds from bed surface observation, Chem. Eng. J. 281 (2015) 109–118, http://dx.doi.org/10.1016/j.cej.2015.06.097.